Transport and Electron Transfer Dynamics in a Polyether-Tailed Cobalt Bipyridine Molten Salt: Electrolyte Effects

Mary Elizabeth Williams, Leslie J. Lyons,† Jeffrey W. Long, and Royce W. Murray*

Kenan Laboratories of Chemistry, University of North Carolina, Chapel Hill, North Carolina 27599-3290, and Department of Chemistry, Grinnell College, Grinnell, Iowa 50112-0806

Received: May 6, 1997[⊗]

Transport, ionic conductivity, and viscosity properties of the metal complex molten salt $[Co(bpy(CO_2MePEG\text{-}350)_2)_3](ClO_4)_2$ (MePEG = monomethyl-terminated polyether, average MW = 350) are strongly affected by dissolution of $LiClO_4$ electrolyte in the melt. The physical self-diffusion of the $[Co(bpy(CO_2MePEG\text{-}350)_2)_3]^{2+}$ and the rate of $[Co(bpy(CO_2MePEG\text{-}350)_2)_3]^{2+/+}$ electron self-exchange are slowed, the melt viscosity increased and ionic conductivity decreased, and thermal activation barriers for all are enhanced by increasing $[LiClO_4]$. Most of the effects are associated with the Li^+ cation/polyether coordination well-known in polymer electrolytes, in which chain cross-linking and a decrease in chain segmental mobility occurs. The $[Co(bpy(CO_2MePEG\text{-}350)_2)_3]^{2+/+}$ electron self-exchange reaction is shown to be adiabatic (kinetic prefactor *ca.* 10^{13} s^{-1}), and modest changes in its rate with $[LiClO_4]$ are caused by changes in the electron transfer barrier energy. The results are used to draw a hierarchy of dynamics in the metal complex melt in which, for $[LiClO_4] = 1.3$ M, the average diffusive jump rate is *ca.* 3 s^{-1}, the average electron hopping rate is *ca.* 2×10^4 s^{-1}, and the rate of short-range motions of the hard metal complex core within its soft polyether shell (producing adjacent core−core contacts) is *ca.* $\geq 10^5$ s^{-1}.

Introduction

Our synthetic work over the past several years[1] has established that a highly viscous, room temperature molecular melt or molten salt is the general consequence of combining oligomeric polyether chains of appropriate length with molecular or ionic species. This tactic of combining materials that are room temperature liquids with ones that are normally crystalline at room temperature has been applied to a number of redox moieties including metal bipyridine complexes, whose self-diffusion and electron transfer dynamics properties can be explored using "solid state microelectrode voltammetry".[2] In a study[1a] of polyether "tailed" Co bipyridine complexes, we established that (i) physical diffusion of the Co(II) complex slows when the attached polyether chain length is shorter, but that Co(II/I) electron self-exchange dynamics were (ii) *independent* of the chain length, (iii) *adiabatic* or nearly so, and (iv) slower than comparable fluid-phase Co(II/I) dynamics substantially because of the larger electron transfer activation barrier energies imposed in the metal complex melts. The voltammetric measurements relied on the intrinsic ionic conductivity of the Co complex melt, which is possible without significant migration effects[1a] because the ClO_4^- counterion is the principal ionic charge carrier.

It is well-known from the polymer electrolyte literature that electrolytes like $LiClO_4$ readily dissolve in polyethers, giving melts with ionic conductivity, viscosity, and solute diffusion rates that vary strongly with the opposing factors, added ionic content *vs* coordinative cross-linking of polyether chains by Li^+/ether oxygen interactions. Having previously exploited these factors in studies of diffusive and electron transfer dynamics of tetracyanoquinodimethane (TCNQ) redox species,[3] we here report their effects on a polyether-tailed Co bipyridine complex, namely $[Co(bpy(CO_2MePEG\text{-}350)_2)_3](ClO_4)_2$,

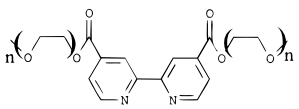

n = 7; MePEG-350

where MePEG-350 is a methyl-terminated polyether with 7 (average) ethylene oxide repeat units. The polyether component of the metal complex melt aids dissolution of $LiClO_4$ electrolyte, which was added in amounts ranging from 0.33 Li^+ to 4.3 Li^+ per Co complex. The results show that these quantities of electrolyte in the $[Co(bpy(CO_2MePEG\text{-}350)_2)_3](ClO_4)_2$ melt produce large changes in its viscosity, ionic conductivity, Co(II) complex physical diffusion, and Co(II/I) complex electron transfer dynamics, as well as in the associated thermal activation parameters. The changes in the Co(II/I) electron transfer dynamics are the smallest, and that reaction retains its apparent adiabaticity. The results will be rationalized into a kinetic hierarchy, within which macroscopic physical diffusion of the metal complex is the slowest and its physical translation on the molecular length scale the fastest, with electron transfers having an intermediate rate.

The rate of macroscopic (*i.e.*, over many molecular length scales) physical diffusion (D_{PHYS}) of the above Co(II) complex in its undiluted melt phase can be resolved from the electron transfer rate constant for the Co(II/I) complex, k_{EX}, by voltammetrically measuring the difference between the diffusion rates for the oxidation (Co(III/II) couple) and reduction (Co(II/I) couple) of the Co(II) complex. This procedure, employed in our previous papers,[1a,b] dates to early work by Buttry and Anson[4] on the $[Co(bpy)_3]^{2+}$ couple in water-swollen Nafion films, and relies on the so-called Dahms−Ruff relation,[5] which in its corrected form is[6]

$$D_{APP} = D_{PHYS} + D_E = D_{PHYS} + k_{EX}\delta^2 C/6 \qquad (1)$$

where D_{PHYS} is the metal complex physical self-diffusion

* Corresponding author.
† Grinnell College.
⊗ Abstract published in *Advance ACS Abstracts,* August 15, 1997.

S1089-5647(97)01519-8 CCC: $14.00

coefficient, D_E is the so-called electron diffusion coefficient, and C and δ are the concentration of and average center-to-center distance between the metal centers, which are evaluated from the melt densities. Use of eq 1 is predicted on the fact that the electron self exchange rate constant for the Co(III/II) couple of $[Co(bpy)_3]^{2+}$ complexes is many orders of magnitude (*ca.* 10^8) slower than that of the Co(II/I) couple.[7] Note that in practical use of eq 1, it is not necessary that the Co(III/II) exchange rate be zero, only that it be more than *ca.* 10-fold smaller than that of the Co(II/I) couple.

Experimental Section

Chemicals. 4-Picoline (Aldrich) and acetonitrile (Fisher) were purified by distillation. Polyethylene glycol monomethyl ether (M_N = 350 MePEG-350, Aldrich) was dried at 70 °C under vacuum for a minimum of 24 h. $Co(ClO_4)_2 \cdot 6H_2O$ (Aldrich) and $LiClO_4$ were stored in a desiccator prior to use. All other chemicals were reagent grade and used as received.

Preparation of Complex. 4-Picoline is catalytically coupled[8] to make 4,4′-dimethyl-2,2′-bipyridine by refluxing with 10% Pd on activated carbon. The dimethyl bpy is then converted to its carboxylic acid[9] and subsequently reacted with thionyl chloride to form the bpy diacid chloride.[10] The acid chloride is then reacted with MePEG-350 in a benzene solution to give the tailed ligand 4,4′-di(polyethylene glycol methyl ether)-2,2′-bipyridine, which is then purified by column chromatography on silica gel as previously described[1a,b] and purity confirmed by ^{1}H NMR.[11] The pure, di-tailed ligand is reacted with $Co(ClO_4)_2 \cdot 6H_2O$ in a methanolic solution to form the $[Co(bpy(CO_2\text{-}MePEG\text{-}350)_2)_3](ClO_4)_2$ complex. Excess ligand is removed by repeated extraction with diethyl ether and purity confirmed by ^{1}H NMR.[12]

Preparation of Metal Complex/Electrolyte Mixtures. The $[Co(bpy(MePEG\text{-}350)_2)_3](ClO_4)_2$ melt is dried thoroughly in a vacuum oven for a minimum of 30 h at 70 °C in order to remove water. A solution of *ca.* 0.045 M $LiClO_4$ in acetonitrile is prepared and the desired aliquot added to the dry Co complex; additional (10−15 mL) acetonitrile is added to completely homogenize the mixture, which is then dried thoroughly of solvent. Solutions of $LiClO_4$ in the MePEG-350 oligomer are prepared analogously.

Electrochemical Measurements. Electrochemical measurements were performed using thoroughly dried, *ca.* 2 mm thick films of the MePEG-350 tailed Co complex melts cast on the platform of a microdisk assembly containing the tips of a 12.2 μm radius Pt electrode, a 26 gauge Pt counter electrode, and a 0.5 mm Ag wire contained within an epoxy cylinder.[13] The surface of the platform was polished with successively smaller grades (to 0.05 μm) of alumina and sonicated in ethanol prior to use. Films were dried at elevated temperatures under vacuum for a minimum of 24 h prior to measurement. Temperature was controlled using a Neslab Model RTE-140 circulating bath and measured with a thermocouple at the cell wall.

Cyclic voltammetric (CV) and potential step chronoamperometric measurements were performed using a home-built low-current potentiostat[14] and locally written computer data acquisition software.[15] CV's were used to determine the peak potentials of the Co(II/I) and (III/II) waves, and potential steps of 300−350 mV from a non-faradaic region to a diffusion-limited potential of the wave were applied for 180−1200 s. Because of the slow diffusion rates in the melts, transport is purely linear diffusion geometry, and the current decay during chronoamperometry is analyzed by the Cottrell equation:[16]

$$I = nFAD^{1/2}C/\pi^{1/2}t^{1/2} \qquad (2)$$

where I is current, n the number of electrons transferred in the reaction, F Faraday's constant, A the microelectrode area, D the diffusion coefficient, and t time in seconds. The time scale of the chronoamperometric measurements was such that even the most slowly diffusing Co(II) complexes were transported over a minimum of 80 nm (*ca.* 50 metal complex diameters) during the experiment; *i.e.*, although diffusion is slow, it is faster than "molecule-scale diffusion".[1f]

Ionic conductivities were measured for *ca.* 2 mm thick films cast onto Pt interdigitated array (IDA) electrodes, generously donated by O. Niwa of Nippon Telephone and Telegraph, with 50 pairs of fingers, each 3 μm wide, 0.1 μm high with 5 μm gaps, and 1 mm long. The cell constant was determined to be 0.1153 cm^{-1} using a solution of known resistance, 1 M $LiClO_4$ in MePEG-2000. The films were dried under vacuum at 50 °C for a minimum of 36 h. Temperature was controlled by a Lakeshore Model 330 autotuning temperature controller. Alternating current (ac) impedance spectroscopy was performed using a Solartron Model 1260 impedance/gain phase analyzer with a SI 1287 electrochemical interface, using a dc bias of 0 V, an ac amplitude of 20 mV, and a frequency range from 1 MHZ to 1 Hz. The resistivity of the film is determined from the intercept of the semicircle on the real axis in the complex impedance plot, and converted to the ionic conductivity using the cell constant of the electrode.

Viscosity Measurements. Films of *ca.* 1 mL of each Co complex/$LiClO_4$ mixture in acetone were evenly cast on the plate of a Brookfield Model DV-III rheometer and placed in a vacuum over at 70 °C to dry for 48 h. Viscosity measurements were made (using Brookfield cone CP-52) under dry nitrogen over several cone rotation rates according the manufacturer's specificiations. Temperature was controlled by a Brookfield circulating bath and measured with a thermocouple housed in the viscometer plate.

Viscosities of the more fluid MePEG-350/$LiClO_4$ mixtures were measured using a Brookfield Model DV-I viscometer (using cone CP-40). The 0.5 mL samples were prepared in the same manner as the Co complex melts and viscosity measurements taken using several shear rates and over a range of temperatures.

Thermal Measurements. Differential scanning calorimetry (DSC) was performed using a Seiko DSC 220-CU instrument with carefully dried, preweighed samples, from −80 to 80 °C at a heating rate of 5 °C/min. The glass transition temperature was determined from the inflection point in the transition and taken as the average value of the heating and cooling curves.

Results

Ionic Conductivity. Room temperature ionic conductivity, σ_{ION}, of the neat Co complex melts, determined by ac impedance spectroscopy, increases with addition of as little as $^1/_3$ equiv of $LiClO_4$ per metal complex (O:Li ratio 126:1), but further additions of $LiClO_4$ produce steadily decreasing ionic conductivities as shown in Figure 1A. Table 1 lists how ionic conductivities observed at 25 °C, and thermal activation parameters ($E_{A,ION}$), depend on $LiClO_4$ concentration. The temperature-dependent conductivity plots are curved when presented as Arrhenius plots over the −20 to 60 °C temperature range (Figure 1B shows examples for different [$LiClO_4$]); for purposes of approximate comparisons with other Arrhenius activation data, activation barriers ($E_{A,ION}$, Table 1) were taken from linear regressions of the upper portion of the temperature range (≥20 °C).[17]

Viscosities. Viscosities, η, of undiluted $[Co(bpy(MePEG\text{-}350)_2)_3](ClO_4)_2$ melts were measured over a range of temper-

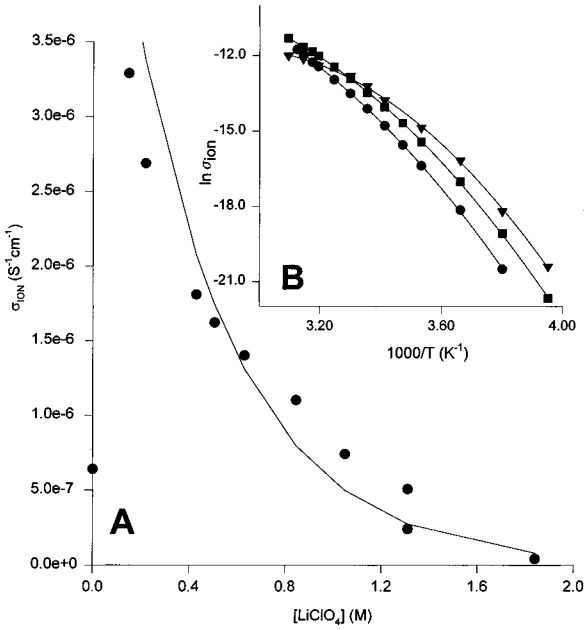

Figure 1. (A) Dependence of σ_{ION} on $LiClO_4$ electrolyte concentration in $[Co(bpy(MePEG350)_2)_3](ClO_4)_2$; (B) corresponding Arrhenius plots for $LiClO_4$ concentrations of 0.403 M (▼), 0.630 M (■), and 1.05 M (●). Lines are VTF fits (see ref 17).

TABLE 1: Ionic Conductivity Measurements for Neat $[Co(bpy(MePEG\text{-}350)_2)_3](ClO_4)_2$ Containing $LiClO_4$

$[LiClO_4]$ (M)	O:Li[a]	σ_{ION} (Ω^{-1} cm^{-1})[b] (25 °C)	$E_{A,ION}$[c] (kJ mol^{-1})	T_G[d] (K)
0		6.4×10^{-7}	48 ± 2	217
0.148	126:1	3.3×10^{-6}	52 ± 3	224
0.219	84:1	2.7×10^{-6}	47 ± 2	227
0.430	42:1	1.8×10^{-6}	57 ± 3	232
0.506	35:1	1.6×10^{-6}	61 ± 3	231
0.630	28:1	1.4×10^{-6}	72 ± 2	231
0.846	21:1	1.1×10^{-6}	80 ± 3	237
1.05	17:1	7.4×10^{-7}	87 ± 4	239
1.31	14:1	5.1×10^{-7}	95 ± 3	244
1.84	10:1	4.2×10^{-8}	131 ± 4	

[a] Ratio of polyether oxygen to Li, where each MePEG-350 tail contains (on average) 7.2 oxygen atoms, and each Co complex contains 43.2 oxygens. [b] Measurement uncertainties are 1−2% throughout. [c] From linear regression for temperatures ≥20 °C. [d] Glass transition temperature from differential scanning calorimetry.

TABLE 2: Viscosity Results for $[Co(bpy(MePEG\text{-}350)_2)_3](ClO_4)_2$ Containing $LiClO_4$

$[LiClO_4]$ (M)	η (cP) (25 °C)	$E_{A,\eta}$[b] (kJ mol^{-1})
0	1.5×10^4	73 ± 1
0.148	3.5×10^4	67 ± 2
0.219	2.8×10^4	69 ± 1
0.430	5.7×10^4	74 ± 2
0.506	1.2×10^5	78 ± 2
0.630	1.9×10^5	80 ± 2
0.846	3.7×10^5	85 ± 3
1.05	5.5×10^5	89 ± 2
1.31	1.5×10^6	97 ± 3
1.84	8.6×10^6	109 ± 4

[a] Average viscosity over a minimum of 6 shear rates. Measurement uncertainties are <1% throughout. [b] From linear regression of Arrhenius plot for temperatures ≥20 °C.

atures and were independent of shear rate.[18] Reported values are averages. Table 2 shows that the room temperature viscosity increases by over 10^2-fold with increasing $LiClO_4$ concentration, displayed in Figure 2A as a plot of fluidity ($1/\eta$). The temperature dependence of melt fluidity at different $[LiClO_4]$, illustrated in Figure 2B, was analyzed as for ionic conductivity.[19]

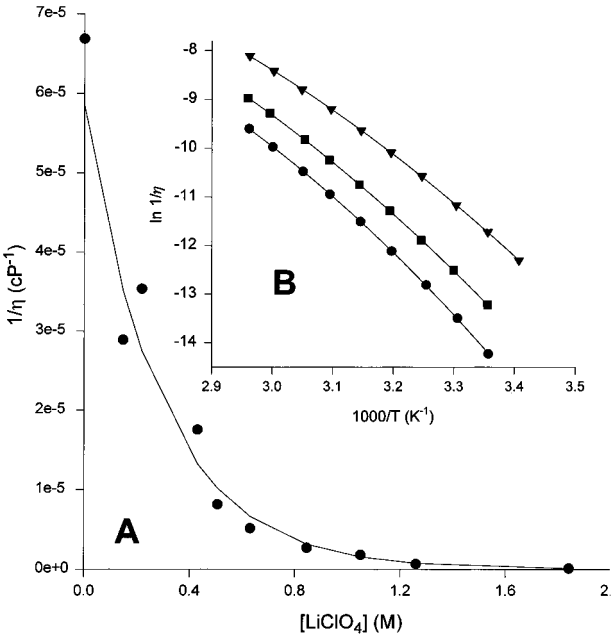

Figure 2. (A) Fluidity ($1/\eta$) of $[Co(bpy(MePEG350)_2)_3](ClO_4)_2$ dependence on $LiClO_4$ electrolyte concentration; (B) corresponding Arrhenius plots of $1/\eta$ for $LiClO_4$ concentration 0.430 M (▼), 0.630 M (■), and 1.05 M (●). Lines are VTF fits (see ref 19).

TABLE 3: Viscosity of MePEG-350 Solutions Containing $LiClO_4$

$[LiClO_4]$ (M)	η[a] (cP) (25 °C)	$E_{A,\eta}$[b] (kJ mol^{-1})
0	25.7	32 ± 1
0.18	33.3	32 ± 1
0.53	50.3	40 ± 2
0.77	70.2	39 ± 1
1.32	181.6	45 ± 2
2.04	533.8	57 ± 2

[a] Average viscosity over a minimum of six shear rates. Measurement are ±1%. [b] From linear regression over a temperature range of ≥20 °C.

The resulting Arrhenius viscosity activation barriers, $E_{A,\eta}$, increase with increasing $[LiClO_4]$ (Table 2).

The viscosity of polyether/electrolyte solutions is well-known to increase with added electrolyte.[20] The specifics of this were examined for solutions of $LiClO_4$ in pure MePEG-350 polyether tail; room temperature viscosity and thermal activation results are given in Table 3. By comparison to Table 2, the viscosities and activation barriers for the $LiClO_4$/MePEG-350 polymer electrolyte are both much smaller than those for the $LiClO_4$-$[Co(bpy(MePEG\text{-}350)_2)_3](ClO_4)_2$ melts, and the viscosities for the metal complex melts also increase much more sharply with increasing $[LiClO_4]$.

Differential Scanning Calorimetry. DSC traces for the $[Co(bpy(MePEG\text{-}350)_2)_3](ClO_4)_2$ melts containing $LiClO_4$ electrolyte show clear glassing and no melting transitions. The absence of melting transitions is favorable since crystallinity in these materials would complicate analysis of the transport data. Values of the glassing temperatures (T_G, Table 1) increase regularly (in fact, linearly, Figure 3) from −55 to −18 °C with increasing electrolyte concentration. A linear relationship has been seen in a variety of polyether mixtures, where T_G typically rises with electrolyte concentration, but begins to level off at O/Li > 15:1.[21]

Diffusion Coefficient Measurements. Cyclic voltammetry of a $[Co(bpy(MePEG\text{-}350)_2)_3](ClO_4)_2$ melt containing added $LiClO_4$ is illustrated in Figure 4. As seen before[1a,d] for such

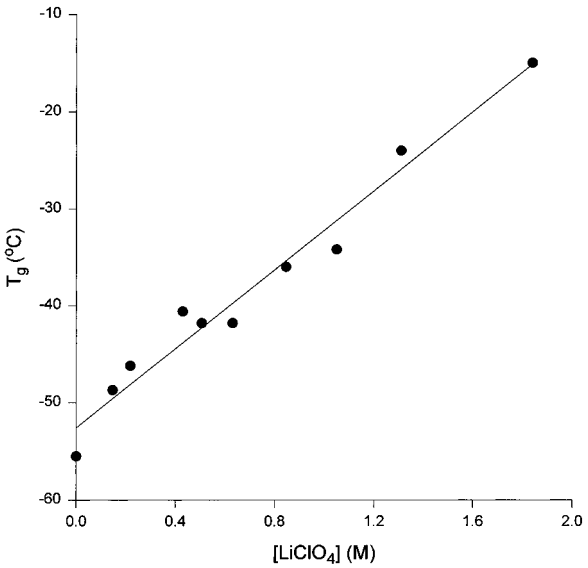

Figure 3. Glass transition temperature, T_G, as a function of $LiClO_4$ concentration in the melt.

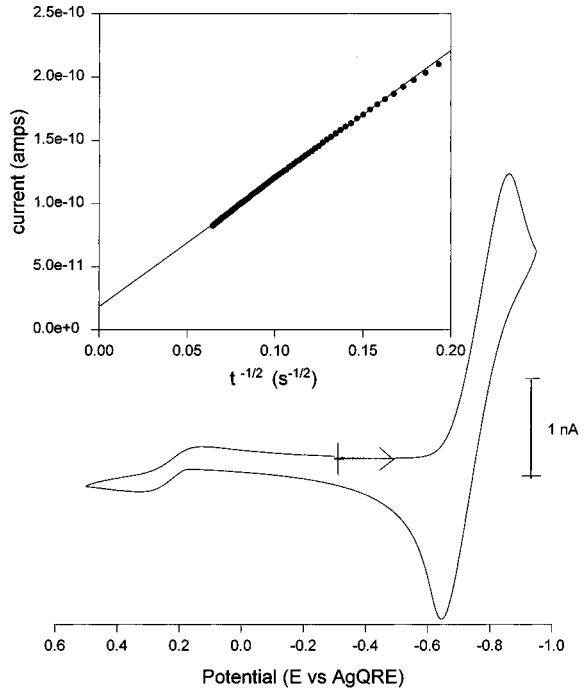

Figure 4. Cyclic voltammogram of neat $[Co(bpy(MePEG350)_2)_3](ClO_4)_2$ containing 0.219 M $LiClO_4$ at a 12.5 μm radius Pt electrode, at 36 °C and a potential scan rate of 10 mV s^{-1}. Inset. Cottrell plot of the Co(III/II) couple (···), eq 2, for potential step on the same sample, with linear regression (—).

melts, currents for the reduction of the complex are much larger than those for its oxidation, meaning that the effective diffusion coefficient derived from Co(III/II) oxidation is less than that from Co(II/I) reduction. Potential step chronoamperometry (Figure 4, inset) was used to measure the diffusion coefficients, which as discussed in reference to eq 1 are labeled respectively D_{APP} (for the Co(II/I) reaction, which is enhanced by Co(II/I) electron self-exchange) and D_{PHYS} (for the Co(III/II) reaction which measures only physical self-diffusion of $[Co(bpy(MePEG\text{-}350)_2)_3]^{2+}$ in the neat melt). The resulting values for D_{PHYS} and D_{APP} at 25 °C, and their difference (D_E, eq 1, Table 4) are plotted in Figure 5 as a function of added $LiClO_4$ concentration. Both D_{PHYS} and D_{APP} increase slightly upon addition of a small $LiClO_4$ concentration and then decrease steadily with increasing $LiClO_4$ concentration. The changes in D_{PHYS} are much larger than those in D_{APP}.

Examples of temperature dependencies of D_{PHYS} and D_E are shown in the Figure 5 insets. The Arrhenius plots for D_{PHYS} are curved whereas those for D_E (and for D_{APP}) are relatively linear, as seen before for Co bipyridine melts.[1a] Table 4 presents activation barriers; those for physical transport of the Co(II) complex are larger than for Co(II/I) electron self-exchange and both increase with electrolyte concentration.

Discussion

Before considering the above results, it is useful to summarize (cartoon in Figure 6) the transport picture of the $LiClO_4$-free $[Co(bpy(MePEG\text{-}350)_2)_3](ClO_4)_2$ melt developed in our previous study:[1a] (i) The metal complex "core" is considered "hard" and nondeformable relative to the shell of polyether chains attached to it. The complex core has a diameter of *ca.* 12 Å (defined by the outer part of the bipyridine rings and ignoring the clefts between ligands), and the MePEG-350 chains, if one imagines them in terms of an increment to the spherical core's diameter, comprise a layer *ca.* 2 Å thick. (ii) Physical self-diffusion of the metal complexes in their pure melts requires pushing relatively bulky molecules past one another (Figure 6A); that the physical diffusion is aided by deformations of the soft polyether shell was inferred[1a] from the substantial increase in D_{PHYS} values for longer attached polyether chain lengths. (iii) Even for the longest polyether chains used, the diffusion coefficient of the ClO_4^- counterion (D_{ClO_4}) exceeded that of the $[Co(bpy(MePEG\text{-}350)_2)_3]^{2+}$ ion; *i.e.*, the ClO_4^- counterion is the principal ionic charge carrier in the pure melt phase. The ClO_4^- counterion presumably resides mainly in and is transported through the soft polyether shells of the metal complexes.

In the present experiments, addition of $LiClO_4$ electrolyte to Figure 6 will increase the population of unassociated ClO_4^- counterions in the melt and should also lead to stronger interactions between $[Co(bpy(MePEG\text{-}350)_2)_3]^{2+}$ ions through Li^+ association with ether dipoles on adjacent complexes. The consequences of such interactions should be manifest in properties like D_{PHYS} and viscosity.

Ionic Conductivities and Ionic Migration Effect. Ionic conductivity reflects a product of ionic population and mobility. In the pure $[Co(bpy(MePEG\text{-}350)_2)_3](ClO_4)_2$ melt, the formal populations of ionic species are known quantities (0.445 M $[Co(bpy(MePEG\text{-}350)_2)_3]^{2+}$ and 0.89 M ClO_4^-), as is the metal complex mobility (by chronoamperometry, $D_{PHYS} = 1.3 \times 10^{-11}$ cm^2/s, Table 4). The Stokes−Einstein relation between diffusivity and ionic conductivity can be used[1a−c] to calculate D_{ClO_4} (3.5×10^{-10} cm^2/s), which leads to a transference number of 0.13 for the Co complex (Table 5). The ClO_4^- counterion is thus the predominant ionic charge carrier. This observation crucially aids assessment of the potential for migration effects (ionic and (*vide infra*) electronic) on values for the transport and electron transfer dynamics. Those dynamics are the main objectives of this study.

The results at very dilute $[LiClO_4]$ sheds particularly useful insight into the behavior of small ions (Li^+ and ClO_4^-) in the $[Co(bpy(MePEG\text{-}350)_2)_3](ClO_4)_2$ melts. Addition of small $[LiClO_4]$ to a $[Co(bpy(MePEG\text{-}350)_2)_3](ClO_4)_2$ melt increases its ionic conductivity (σ_{ION}, Table 1). For the smallest added $[LiClO_4]$ (0.148 M), while the nominal population of small ions (Li^+ and ClO_4^-) is increased by 33%, the value of σ_{ION} is increased 5-fold. σ_{ION} is less at higher electrolyte concentrations, so that at $[LiClO_4] = 0.43$ M, while the small ion population is double that of a pure $[Co(bpy(MePEG\text{-}350)_2)_3](ClO_4)_2$ melt, the value of σ_{ION} is increased by only 3-fold

TABLE 4: Transport Measurements in Neat [Co(bpy(MePEG-350)$_2$)$_3$](ClO$_4$)$_2$ Melts Containing LiClO$_4$ Electrolyte

concn of LiClO$_4$ (M)	concn of Co (M)[a]	D_{PHYS}(25 °C)[b] Co(III/II) (cm^2 s^{-1})	D_{APP}(25 °C)[b] (CoII/I) (cm^2 s^{-1})	D_E (25 °C)[c] Co(II/I) (cm^2 s^{-1})	$E_A(D_{PHYS})$ (kJ mol^{-1})	$E_A(D_E)$ (kJ mol^{-1})	$k°_{EX}$[e] Co(II/I) (M^{-1} s^{-1})
0	0.445	1.3×10^{-11}	1.5×10^{-9}	$(1.5 \pm 0.1) \times 10^{-9}$	73 ± 2	37 ± 1	$(6 \pm 2) \times 10^{12}$
0.148	0.440	1.9×10^{-11}	2.2×10^{-9}	$(2.2 \pm 0.1) \times 10^{-9}$	72 ± 2	39 ± 1	$(1 \pm 0.9) \times 10^{13}$
0.219	0.438	2.0×10^{-11}	1.9×10^{-9}	$(1.9 \pm 0.1) \times 10^{-9}$	79 ± 1	39 ± 1	$(7 \pm 3) \times 10^{12}$
0.430	0.430	9.5×10^{-12}	1.0×10^{-9}	$(1.0 \pm 0.1) \times 10^{-9}$	80 ± 1	47 ± 1	$(2 \pm 1) \times 10^{14}$
0.506	0.422	8.7×10^{-12}	1.1×10^{-9}	$(1.1 \pm 1) \times 10^{-9}$	80 ± 2	48 ± 3	$(1 \pm 0.9) \times 10^{14}$
0.630	0.422	5.5×10^{-12}	7.4×10^{-10}	$(7.4 \pm 0.2) \times 10^{-10}$	79 ± 3	47 ± 2	$(8 \pm 4) \times 10^{13}$
0.846	0.423	1.8×10^{-12}	5.3×10^{-10}	$(5.3 \pm 0.1) \times 10^{-10}$	93 ± 2	48 ± 1	$(9 \pm 4) \times 10^{13}$
1.05	0.425	6.0×10^{-13}	3.0×10^{-10}	$(3.0 \pm 0.1) \times 10^{-10}$	101 ± 3	49 ± 2	$(1 \pm 0.9) \times 10^{13}$
1.31	0.425	7.0×10^{-14}	1.0×10^{-10}	$(1.2 \pm 0.1) \times 10^{-10}$	115 ± 4	58 ± 2	$(9 \pm 5) \times 10^{14}$

[a] Concentration from density measurements: $\rho = 1.30$ g/mL for 0 M LiClO$_4$; 1.30 g/mL for 0.219 M LiClO$_4$; 1.286 g/mL for 0.506 M LiClO$_4$; 1.34 g/mL for 0.846 M LiClO$_4$. [b] From chronoamperometry. Measurement uncertainties typically ±5−10% or lower. [c] $D_E = D_{APP} - D_{PHYS}$, eq 1. [d] From linear regression for temperatures ≥20 °C. [e] $k°_{EX} = 6D°_E/\delta^2 C$, where $D°_E$ is the value of D_E at the intercept of the Arrhenius plot. δ is ≈15.5 Å, taken from the molecular volume assuming packed cubes, using the above values for density.

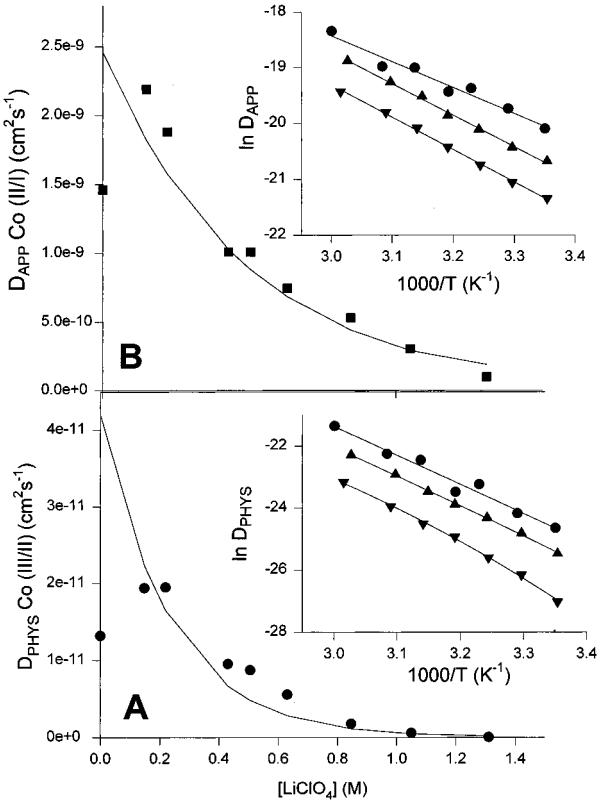

Figure 5. (A) Dependence of D_{PHYS}(CoIII/II) on [LiClO$_4$] and (inset) Arrhenius plots of D_{PHYS} for neat [Co(bpy(MePEG350)$_2$)$_3$](ClO$_4$)$_2$ containing 0.219 M LiClO$_4$ (●), 0.506 M LiClO$_4$ (▲), and 0.846 M LiClO$_4$ (▼); (B) dependence of D_E(CoII/I) versus [LiClO$_4$] and (inset) Arrhenius plots of D_E for neat [Co(bpy(MePEG350)$_2$)$_3$](ClO$_4$)$_2$ containing 0.219 M LiClO$_4$ (●), 0.506 M LiClO$_4$ (▲), and 0.846 M LiClO$_4$ (▼). Lines are guide to eye only.

relative to the pure melt. These comparisons show that in small added amounts, the mobility of added ClO_4^- is much larger than that of the original ClO_4^- counterions of a [Co(bpy-(MePEG-350)$_2$)$_3$](ClO$_4$)$_2$ melt. This strongly suggests that *ion pairing occurs in the pure melt between the metal cation and its ClO$_4^-$ counterions*. It is pertinent to note that the presence of ion pairing in the pure melt results in an *underestimation* of D_{ClO_4}.

At even higher concentrations, the Li^+ ions (as expected) strongly counteract the increase in total small ion population by lowering the small ion mobility, causing an overall decrease in σ_{ION} with increasing [LiClO$_4$]. The change in small ion mobility probably involves both restraint of polyether chain flexibility and the introduction of polyether/Li^+/polyether interactions that induce Co complex association.

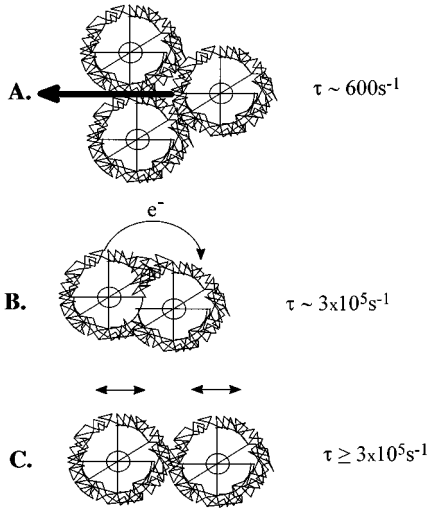

Figure 6. Cartoon showing the relative timescales of (A) physical self-diffusion of tailed Co(II) molecules, (B) electron self-exchange between Co(II/I) metal centers, and (C) inferred mobility of the Co metal centers within their polyether "shell". Times are for 0 M LiClO$_4$.

The Stokes−Einstein relation can be used to estimate D_{ClO_4} also in the LiClO$_4$-containing melts, for which it is written[22]

$$\sigma_{ION} = \frac{F^2}{RT}(z_{Co}{}^2 D_{Co} C_{Co} + z_{Li}{}^2 D_{Li} C_{Li} + z_{ClO_4}{}^2 D_{ClO_4} C_{ClO_4}) \quad (3)$$

where σ_{ION} values are given in Table 1, z is the charge on each ion, and D and C are the diffusion coefficient and concentration of the indicated species, respectively. An assumption is necessary, and was made in two ways: (a) Assume that the mobility of Li^+ equals that of the metal complex cation (because of its association with the polyether), *i.e.*, $D_{Li} = D_{Co} = D_{PHYS}$. Taking the latter parameter from Table 4, eq 3 leads to values of D_{ClO_4} as in Table 5.[23] (b) Assume that Li^+ and ClO_4^- have the same mobility (*i.e.*, $D_{Li} = D_{ClO_4}$; this assumption is less plausible given the Li^+/polyether association), which yields diffusivities labeled as $D^*_{ClO_4}$ in Table 5. Comparison of D_{ClO_4} and $D^*_{ClO_4}$ (Table 5) shows that the two assumptions produce similar ClO_4^- diffusivities and that in all cases $D_{ClO_4} > D_{PHYS}$ by even larger amounts than in the pure [Co(bpy(MePEG-350)$_2$)$_3$](ClO$_4$)$_2$ melt.

The above results can be used to evaluate possible errors in the measured D_{PHYS} values due to ionic migration of the [Co-(bpy(MePEG-350)$_2$)$_3$]$^{2+}$. The criterion for the absence of such migration is a small or negligible transference number for the metal complex; that parameter can be calculated from[24]

TABLE 5: Analysis of Perchlorate Diffusion, Transference Numbers, and Migration Effects

	assume $D_{Li} = D_{Co}$			assume $D_{Li} = D_{ClO_4}$				
[$LiClO_4$] (M)	D_{ClO_4}[a] ($cm^2\ s^{-1}$) (25 °C)	D_{ClO_4}/D_E	$D_{E,COR}$[b] ($cm^2\ s^{-1}$) (25 °C)	$D^*_{ClO_4}$[c] ($cm^2\ s^{-1}$) (25 °C)	D_{ClO_4}/D_E	$D^*_{E,COR}$[d] ($cm^2\ s^{-1}$) (25 °C)	t_{Co}[e]	$k_{EX,COR}$[f] ($M^{-1}\ s^{-1}$) (25 °C)
0	3.5×10^{-10}	0.24 ± 0.02	1.2×10^{-9}	3.5×10^{-10}	0.24 ± 0.02	1.2×10^{-9}	0.13 ± 0.05	$6.8\ (\pm 0.5) \times 10^5$
0.148	1.4×10^{-9}	0.66 ± 0.05	1.9×10^{-9}	1.1×10^{-9}	0.53 ± 0.04	1.9×10^{-9}	0.039 ± 0.004	$1.1\ (\pm 0.1) \times 10^6$
0.219	1.0×10^{-9}	0.55 ± 0.06	1.7×10^{-9}	7.8×10^{-10}	0.41 ± 0.03	1.6×10^{-9}	0.048 ± 0.004	$9.4\ (\pm 0.3) \times 10^5$
0.430	5.4×10^{-10}	0.54 ± 0.05	8.7×10^{-10}	3.6×10^{-10}	0.36 ± 0.02	8.7×10^{-10}	0.034 ± 0.003	$5.1\ (\pm 0.4) \times 10^5$
0.506	4.4×10^{-10}	0.43 ± 0.05	9.2×10^{-10}	2.9×10^{-10}	0.28 ± 0.03	9.1×10^{-10}	0.034 ± 0.004	$5.5\ (\pm 0.5) \times 10^5$
0.630	3.4×10^{-10}	0.47 ± 0.04	6.4×10^{-10}	2.2×10^{-10}	0.29 ± 0.02	6.2×10^{-10}	0.025 ± 0.002	$3.8\ (\pm 0.3) \times 10^5$
0.846	2.3×10^{-10}	0.43 ± 0.05	4.6×10^{-10}	1.4×10^{-10}	0.26 ± 0.02	4.5×10^{-10}	0.010 ± 0.02	$2.7\ (\pm 0.3) \times 10^5$
1.05	1.2×10^{-10}	0.40 ± 0.04	2.6×10^{-10}	7.4×10^{-11}	0.24 ± 0.01	2.6×10^{-10}	0.051 ± 0.04	$1.5\ (\pm 0.2) \times 10^5$
1.31	7.8×10^{-11}	0.78 ± 0.06	9.0×10^{-11}	4.4×10^{-11}	0.44 ± 0.04	8.7×10^{-11}	0.0088 ± 0.02	$5.3\ (\pm 0.5) \times 10^4$

[a] D_{ClO_4} is the diffusion coefficient of the ClO_4^- counterion, calculated assuming $D_{Co} = D_{Li} = D_{PHYS}$. [b] The electron diffusion coefficient for Co(II/I), corrected for electronic migration effects using the D_{ClO_4} value calculated assuming $D_{Li} = D_{Co}$. [c] $D^*_{ClO_4}$ diffusion coefficient calculated for ClO_4^-, assuming $D_{Li} = D_{ClO_4}$. [d] $D_{E,COR}$ determined using $D^*_{ClO_4}$. [e] The transference number of the Co^{2+} metal complex. [f] $k_{EX,COR}$ calculated from $D_{E,COR} = k_{EX,COR}\delta^2 C/6$.

$$t_{Co} = \frac{z_{Co}^2 D_{Co} C_{Co}}{z_{Co}^2 D_{Co} C_{Co} + z_{Li}^2 D_{Li} C_{Li} + z_{ClO_4}^2 D_{ClO_4} C_{ClO_4}} \quad (4)$$

The t_{Co} values given in Table 5 are *independent* of assumptions made in calculating D_{ClO_4} and show that, in the presence of added electrolyte, ionic migration of $[Co(bpy(MePEG\text{-}350)_2)_3]^{2+}$ is entirely negligible. In the pure melt, the t_{Co} value indicates that a minor ionic migration effect may occur, which would depress the apparent D_{PHYS}. Its elimination by the addition of even a small [$LiClO_4$] may be responsible for the small increase in D_{PHYS} seen at the lowest [$LiClO_4$] in Table 4.

Consideration of Physical Diffusion and Viscosity Measurements. It is well-known[20b] that for linear polyethers, viscosity increases and chain diffusivity decreases with increasing chain length and electrolyte concentration (*i.e.*, $LiClO_4$). The viscosity change, illustrated for the MePEG-350 polyether tail in Table 3, is classically explained in terms of cross-linking by Li^+ cation/polyether oxygen associations that reduce the chains' segmental mobility.

In the $[Co(bpy(CO_2MePEG\text{-}350)_2)_3](ClO_4)_2$ melts, as compared to linear polyethers, the effect of [$LiClO_4$] is greatly magnified and that of polyether tail chain length is actually opposite in direction. In a previous study,[1a] a 4-fold increase in polyether tail length caused a *ca.* 10^3-fold *decrease* in viscosity and a *ca.* 10^3-fold *increase* in D_{PHYS}. In this study, the viscosity of $[Co(bpy(CO_2MePEG\text{-}350)_2)_3](ClO_4)_2$ melts (Table 2) increases far more with added [$LiClO_4$] than is the case for MePEG-350 tail alone (Table 3), and the physical diffusivity D_{PHYS} of $[Co(bpy(CO_2MePEG\text{-}350)_2)_3]^{2+}$ decreases by a roughly equivalent amount. The activation barriers for η and D_{PHYS} of the $[Co(bpy(CO_2MePEG\text{-}350)_2)_3](ClO_4)_2$ melt (Figure 7) and η of MePEG-350 all increase with [$LiClO_4$]; the former are roughly equal and are over twice that in MePEG-350 (Table 3).

Changes in viscosity and D_{PHYS} in $[Co(bpy(CO_2MePEG\text{-}350)_2)_3](ClO_4)_2$ melts with chain length[1a] and [$LiClO_4$] are clearly dominated by the presence of the hard metal complex core. Undoubtedly, phenomena known from classical, polymer electrolytes operate in these melts; *i.e.*, there is cross-linking and reduced chain segmental mobility due to Li^+/polyether association. However, the attachment of the polyether chains to the metal complexes allows the same Li^+/polyether associations to generate cross-linkages between very bulky entities (*i.e.*, the metal complexes); we presume this to be the source of the enhanced [$LiClO_4$] effect on η and D_{PHYS} and of the large observed barrier energetics (Figure 7). That is, the present results affirm the cartoon of Figure 6A, that physical transport involves deformations of the soft polyether shells of the bulky metal complex core and of its neighbors, and when these deformations are sterically insufficient (*e.g.*, Figure 6A) also requires displacements of neighbor complex cores.

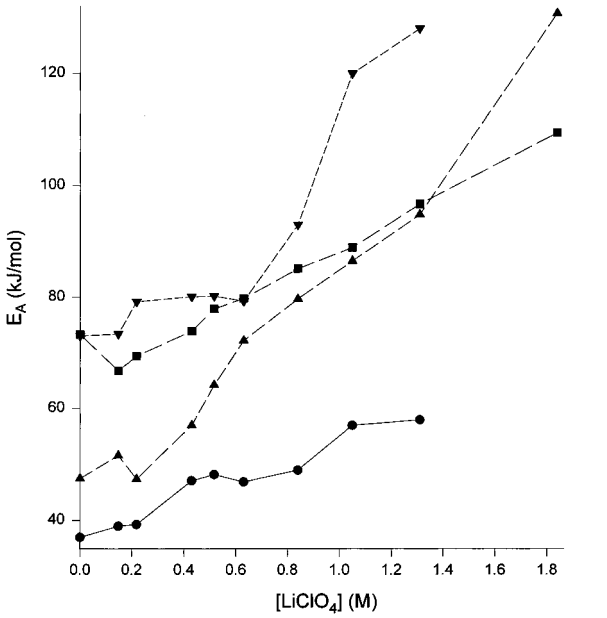

Figure 7. Activation barrier for σ_{ION} (▲), η (■), D_{PHYS} (▼), and D_E (●) for the neat $[Co(bpy(MePEG350)_2)_3](ClO_4)_2$ melts versus $LiClO_4$ concentration.

We observe in passing that comparisons of the present and previous[1a] data to the Stokes−Einstein equation[25]

$$D = kT/6\pi\eta R_H \quad (5)$$

where k is Boltzmann's constant and R_H the hydrodynamic radius of a diffusing molecule, show very roughly the predicted inverse relationship between viscosity and physical diffusion, but produce R_H values much larger than are physically reasonable.[26] The adherence to eq 5 is thus phenomenological only (as been before in analogous measurements)[27] but nonetheless implies that physical displacement of a metal complex unit involves widespread cooperative motions of its neighbors. Given the parameters of Figure 6A, this is intuitively plausible.

Consideration of Electron Transfer Results. Applications of eq 1 to the D_{PHYS}(Co(III/II)) and D_{APP}(Co(II/I)) results of Table 4 leads values of D_E as in Table 4 and following a minor (*ca.* 20%) correction for electronic migration (*vide infra*) to the $D_{E,COR}$ and associated rate constant $k_{EX,COR}$ values in Table 5. Electron transfer activation barriers, $E_A(D_E)$, and intercepts, k°_{EX}, obtained from the temperature dependence of D_E are given in Table 4. We proceed next to an analysis of these results.

Consider first the Arrhenius plot intercepts $k°_{EX}$ in Table 4. While there is perhaps an order-of-magnitude uncertainty due to extrapolation from the relatively short temperature interval studied, it is obvious that $k°_{EX}$ lies near 10^{13} M^{-1} s^{-1}, with no discernible trend with [$LiClO_4$]. The equation for a bimolecular electron transfer reaction is[28]

$$k_{EX} = K_A \kappa \nu \exp[-\Delta G^*/k_B T] \quad (6)$$

where the reorganizational barrier energy $\lambda = 4\Delta G^* \approx 4E_A$, K_A is the donor−acceptor precursor complex formation constant, ν the frequency factor, and κ the electronic factor or transmission coefficient. The value of K_A is near unity[29] so that $k°_{EX}$ in Table 4 can be equated with $\kappa\nu$ of eq 6. A reaction with $\kappa\nu \approx 10^{13}$ s^{-1} is considered to be adiabatic,[28] so this result means that the Co(II/I) electron transfers proceed with little if any distance-imposed tunnelling barrier. That is, the soft polyether shells do not prevent the metal complex cores from *coming into more or less intimate contact at some frequency equal to or larger than the frequency at which electron transfers occurs*. This conclusion was drawn in the previous paper[1a] based on an analogous observation as well as the finding that electron transfer rates were independent of the attached polyether chain length.

The Co(II/I) reaction is self-exchange so that the reaction entropy and entropy of activation are zero,[7,28,30] meaning that activation barriers $E_A(D_E)$ in Table 4 can be equated (neglecting $\Delta S^{\ddagger}_{\lambda}$)[30] with the free energy of activation ΔG^* of eq 6.[28b] Table 4 shows that these values increase modestly with increased [$LiClO_4$], although not nearly as dramatically as those for D_{PHYS}, η and σ_{ION} (Figure 7). Given the rough constancy of $k°_{EX}$, the *ca.* 10-fold decrease in the room temperature rate constant $k_{EX,COR}$ (Table 5) can thus be assigned to the increase in electron transfer energy barrier. The size of ΔG^*, as discussed before,[1a] is much larger than can be rationalized on the basis of a classical "outer sphere" reorganizational barrier of magnitude (*ca.* 9 kJ/mol) appropriate for electron transfer in an ether solvent environment. Possible reasons for the enhanced barrier energy discussed in the previous paper[1a] are, in summary (i) a peculiar "inner sphere-like" barrier term occassioned by the linkage between the bpy ligand and its "ether solvent shell", or (ii) a thermal barrier associated with reorientation dynamics of the ether dipoles in the "solvent shell" (*i.e.*, what is usually called solvent dynamics[31,32]). While the present effects of added [$LiClO_4$] on the electron transfer dynamics are consistent with the previous results,[1a] they do not serve to further elucidate the origin of the large electron transfer energy barrier. Understanding this effect is central to a fuller analysis of the general result[33] that room temperature electron self-exchange (hopping) rates are depressed in solid and semisolid materials, relative to those of the same redox couple reactants in dilute, fluid solutions.

In order to compare the rates of diffusive and electron-hopping events, it is instructive to summarize the experimental findings in terms of time scales. First, the electron-hopping *rates* ($k_{EX}C$) in [Co(bpy(CO_2MePEG-350)$_2$)$_3$](ClO_4)$_2$ melts containing 0 and 1.3 M $LiClO_4$ electrolyte are 3×10^5 and 2×10^4 s^{-1}, respectively. The physical diffusion hopping rate (an average of multiple hops, which is what D_{PHYS} measures) can be estimated from D_{PHYS}/δ^2 as 6×10^2 and 3 s^{-1}, respectively, based on $\delta = 1.5$ nm (a metal complex diameter). The electron-hopping frequency is thus 500- to 7000-fold faster than the average diffusive jump frequency, respectively, and the difference is magnified in the electrolyte-containing melts. Thus, *the electron-hopping rate does not scale linearly with the diffusive jump rate.*

The adiabacity of the Co(II/I) electron transfer reaction means that short-range motions of the metal complexes within their polyether shell (Figure 6C), to and from one another, occur on time scales at least equal to and probably faster than the electron transfers, i.e., $\geq 3 \times 10^5$ and $\geq 2 \times 10^4$ s^{-1} in [Co(bpy(CO_2-MePEG-350)$_2$)$_3$]ClO_4)$_2$ melts containing 0 and 1.3 M $LiClO_4$ electrolyte, respectively. A hierarchy of the dynamics in the [Co(bpy(CO_2MePEG-350)$_2$)$_3$](ClO_4)$_2$ melts can thus be written as in the cartoon of Figure 6.

Consideration of Electronic Migration. A complete analysis of electron transfer dynamics using eq 1 requires comparison of the electron diffusion coefficient D_E with that of the charge-compensating counterion D_{ClO_4}. While at one point a slowly diffusing counterion was thought to be rate-determining on the electron-hopping transport rate,[34] *i.e.*, that a small D_{ClO_4} would depress D_E, it is now appreciated that the actual effect is the opposite: a small D_{ClO_4} *enhances* D_E[35] because a slowly diffusing counterion causes an electrical gradient to form, causing an acceleration of the electron hopping reaction. The maximum effect is less than *ca.* 10-fold. The evaluated D_{ClO_4} values were applied to the theory developed by Saveant,[35] producing the corrected values of D_E (Table 5, $D_{E,COR}$; corrections based on $D^*_{ClO_4}$ are given as $D^*_{E,COR}$) and of self-exchange rate constants (Table 5, $k_{EX,COR}$).[36] The calculations show that electronic migration enhanced the measured rates by a minor *ca.* 1.3-fold factor. The observed 15-fold decrease in $k_{EX,COR}$ with increasing [$LiClO_4$] is thus not associated with electronic migration and must reflect the dependence of electron transfer energy barrier on the changing melt environment as disussed above.

Acknowledgment. This work was funded in part by grants from the Department of Energy and the National Science Foundation. L.J.L acknowledges sabbatical leave support from Grinnell College.

Supporting Information Available: Three tables, giving fits of VTF equation (see ref 18) of ionic conductivity and viscosity of metal complex melts, and of viscosity of MePEG-350, as a function of [$LiClO_4$] (3 pages). See any current masthead page for ordering and Internet access instructions.

References and Notes

(1) (a) Williams, M. E.; Masui, H.; Long, J. W.; Malik, J.; Murray, R. W. *J. Am. Chem. Soc.* **1997**, *119*, 1997. (b) Long, J. W.; Velasquez, C. S.; Murray, R. W. *J. Phys. Chem.* **1995**, *100*, 5492. (c) Masui, H.; Murray, R. W., manuscript in preparation. (d) Velasquez, C. S.; Hutchinson, J. E.; Murray, R. W. *J. Am. Chem. Soc.* **1993**, *115*, 7896. (e) Hatazawa, T.; Terrill, R. H.; Murray, R. W. *Anal. Chem.* **1996**, *68*, 597. (f) Poupart, M. W.; Velasquez, C. S.; Hassett, K.; Porat, Z.; Haas, O.; Terrill, R. H.; Murray, R. W. *J. Am. Chem. Soc.* **1994**, *116*, 1165. (g) Terrill, R. H.; Hatazawa, T.; Murray, R. W. *J. Phys. Chem.* **1995**, *99*, 16676.

(2) Longmire, M. L.; Watanabe, M.; Zhange, H.; Wooster, T. T.; Murray, R. W. *Anal. Chem.* **1990**, *62*, 747.

(3) Wooster, T. T.; Watanabe, M.; Murray, R. W. *J. Phys. Chem.* **1992**, *96*, 5886.

(4) Buttry, D. A.; Anson, F. C. *J. Am. Chem. Soc.* **1983**, *105*, 685.

(5) (a) Ruff, I.; Botar, L. *J. Chem. Phys.* **1985**, *83*, 1292. (b) Ruff, I.; Botar, L. *Chem. Phys. Lett.* **1986**, *126*, 348. (c) Ruff, I.; Botar, L. *Chem. Phys. Lett.*, **1988**, *149*, 99. (d) Dahms, H. *J. Phys. Chem.* **1968**, *72*, 362. (e) Ruff, I.; Friedrich, V. J. *J. Phys. Chem.* **1971**, *75*, 3297. (f) Ruff, I.; Friedrich, V. J.; Demeter, K.; Csaillag, K. *J. Phys. Chem.* **1971**, *75*, 3303.

(6) Majda, M., *Molecular Design of Electrode Surfaces*; Murray, R. W., Ed.; John Wiley & Sons: New York, 1992; p 159.

(7) Sutin, N.; Brunschwig, B. S.; Creutz, C.; Winkler, J. R. *Pure Appl. Chem.* **1988**, *60*, 1817.

(8) Sasse, W. H. F.; Whittle, C. P. *J. Am. Chem. Soc.* **1961**, *83*, 1347.

(9) Sprintschnik, G.; Sprintschnik, H. W.; Kirsch, P. P.; Whitten, D. G. *J. Am. Chem. Soc.* **1977**, *99*, 4947.

(10) Evers, R. C.; Moore, G. J. *J. Polym. Sci.* **1986**, *24*, 1863.

(11) The protons on the first ethylene oxide monomer unit (*i.e.*, adjacent to the ester linkage) are shifted slightly downfield, allowing their integration apart from the remainder of the polymer chain. The ratio of the area of these first four protons on the chain to that for the bipyridine protons is 4:3 for the pure, di-tailed ligand.

(12) (a) Crooker, J. C., University of North Carolina at Chapel Hill, unpublished results, 1995. (b) The lack of the bipyridine proton peaks (between 7.5 and 9.5 ppm) in the ^{1}H NMR spectrum confirms the absence of uncomplexed ligand in the melt.

(13) (a) Watanabe, M.; Wooster, T. T.; Murray, R. W. *J. Phys. Chem.* **1991**, *95*, 45. (b) Wooster, T. T.; Longmire, M. L.; Watanabe, M.; Murray, R. W. *J. Phys. Chem.* **1991**, *95*, 5315.

(14) Woodward, S., University of North Carolina Department of Chemistry Electronics Consultant, design and construction of the potentiostat.

(15) Terrill, R. H., University of North Carolina, unpublished.

(16) Bard, A. J.; Faulkner, L. R. *Electrochemical Methods*; John Wiley & Sons: New York, 1980; p 143.

(17) (a) Grey, F. M. *Solid Polymer Electrolytes, Fundamentals and Technological Applications*; VCH Publishers, Inc.: New York, 1991. (b) The activation data were also fit to the Vogel−Tamman−Fulcher (VTF) equation[19a]

$$\sigma_{\mathrm{ION}} = \frac{A'}{T^{1/2}} \exp\left[\frac{-E_{\mathrm{A}}}{R(T - T_0)}\right]$$

where T_0 is the reduced temperature and A' is a preexponential term related to the number of charge carriers. This relation is commonly applied to ionic conductivities of polyether-based polymer electrolyte systems.[17a] Data are reported in Supporting Information. The substantial scatter in $E_{\mathrm{A,ION}}$(VTF) and T_0 results is probably due to the relatively short temperature range employed; trends with $LiClO_4$ concentration are accordingly hard to discern. The Arrhenius energy barriers, however, show an obvious increase with increasing $LiClO_4$ concentration.

(18) For example, for the 0.506 M $LiClO_4$ melt at 40 °C, the measured viscosity was 23 985, 23 985, 24 011, 24 055, and 24 025 cP at rotation rates of 50, 60, 75, 85, and 100 rpm. For the 1.05 M $LiClO_4$ melt at 61 °C, the viscosity was 10 774, 10 747, 10 800, 10 774, 10 726, and 10 747 cP at rotation rates of 50, 75, 75, 100, 125, and 150 rpm.

(19) VTF activation barriers and reduced temperature, $E_{A,\eta}$(VTF) and T_0, are given in Supporting Information. T_0 seems to be independent of [$LiClO_4$] while $E_{A,\eta}$(VTF) increases with increasing [$LiClO_4$].

(20) (a) Pyati, R.; Murray, R. W. *J. Am. Chem. Soc.* **1996**, *118*, 1743. (b) Hara, M. In *Polyelectrolytes*; Hara, M., Ed.; Marcel Dekker, Inc.: New York: 1993.

(21) (a) Cruickshank, J.; Hubbard, H. C. St. A.; Boden, N.; Ward, I. M. *Polymer* **1995**, *36*, 3779. (b) See also ref 7−10 in ref 21a.

(22) Reference 16, pp 227−231.

(23) This analysis ignores the formation of ion pairs and aggregates in the melt and may underestimate D_{ClO_4}.

(24) Reference 16, p 123.

(25) Atkins, P. W. *Physical Chemistry*, 4th ed.; W. H. Freeman & Co.: New York, 1990.

(26) For example, using D_{PHYS} (Table 4) and η (Table 2), hydrodynamic radii, R_{H}, were 40 and 207 Å in the 0.403 and 1.31 M $LiClO_4$ melts, respectively.

(27) Haas, O.; Velázquez, C. S.; Porat, Z.; Murray, R. W. *J. Phys. Chem.* **1995**, *99* 15279.

(28) (a) Marcus, R. A.; Sutin, N. *Biochim. Biophys. Acta* **1985**, *811*, 265. (b) Marcus, R. A.; Siddarth, P. Photoprocesses. In *Transition Metal Complexes, Biosystems, and Other Molecules*; Kochanski, E., Ed.; Kluwer Academic Publishers: Dordrecht, The Netherlands, 1992. (c) Sutin, N. *Acc. Chem. Res.* **1982**, *15*, 275. (d) Sutin, N. *Prog. Inorg. Chem.* **1983**, *30*, 441.

(29) The work terms are ignored in the calculation of K_{A} and in the statement regarding activation entropy since the reacting molecules are essentially in contact in the undiluted melt. Based on the equation $K_{\mathrm{A}} = 4\pi N_{\mathrm{A}} \bar{r}^2 \delta\bar{r}/10^3$, where the center-to-center distance, $\bar{r}$, is taken as 15.5 and $\delta\bar{r}$ is taken as 0.8,[28c] and K_{A} is calculated to be ~1 M^{-1}.

(30) Newton, M. D.; Sutin, N. *Annu. Rev. Phys. Chem.* **1984**, *35*, 437.

(31) (a) Weaver, M. J. *Chem. Rev.* **1992**, *92*, 463. (b) Fawcett, W. R.; Opallo, M. *Angew. Chem., Int. Ed. Eng.* **1994**, *33*, 2131. (c) Heitele, H. *Angew. Chem., Int. Ed. Eng.* **1993**, *32*, 359.

(32) See footnote 29 in ref 1a.

(33) Terrill, R. H.; Murray, R. W. In *Molecular Electronics*; Jortner, J., Ratner, M. A., Eds.; IUPAC Informal Series Chemistry for the 21st Century, Monographs; Blackwell Science: New York, in press.

(34) Chen, X.; He, P.; Faulkner, L. R. *J. Electroanal. Chem.* **1987**, *222*, 223.

(35) Andrieux, C. P.; Saveant, J.-M. *J. Phys. Chem.* **1988**, *92*, 6761.

(36) The calculated values of $k_{\mathrm{EX,COR}}$ using $D_{\mathrm{E,COR}}$ and $D^*_{\mathrm{E,COR}}$ are essentially equivalent within the stated experimental uncertainties.